Effect of lanthanum doping on tetragonal-like $BiFeO_3$ with mixed-phase domain structures

Lu You,[1,*] Petrus Caesario,[1] Liang Fang,[1,2] Peng Ren,[1] Le Wang,[1] Yang Zhou,[1] Alexei Gruverman,[3] and Junling Wang[1,†]

[1]*School of Materials Science and Engineering, Nanyang Technological University, Singapore 639798, Singapore*

[2]*College of Physics, Optoelectronics and Energy, Soochow University, Suzhou 215006, People's Republic of China*

[3]*Department of Physics and Astronomy, University of Nebraska—Lincoln, Lincoln, Nebraska 68588, USA*

(Received 13 August 2014; revised manuscript received 18 September 2014; published 31 October 2014)

The recent discoveries of both chemical-driven and strain-driven morphotropic phase boundaries (MPBs) in $BiFeO_3$ (BFO) thin films have opened up new horizons in developing high-performance lead-free piezoelectrics. An attempt to bridge these two MPBs is made by doping La into highly strained BFO thin films with the coexistence of tetragonal-like and rhombohedral-like phases. The structural, morphological, and ferroelectric properties of such films are investigated. It is observed that La doping changes the energy landscape between the tetragonal-like and the rhombohedral-like polymorphs due to the chemical pressure imposed by the La substitution. Polar instability is found upon increasing La doping for the in-plane polarization component, which correlates with the vanishing of in-plane ferroelectric domain structures. The transition sequence of the in-plane ferroelectric polarization resembles that previously reported for the bulklike rhombohedral phase of BFO under continuous La doping, indicating the universality of the chemical-alloying effect on the ferroelectric order.

DOI: 10.1103/PhysRevB.90.134110 PACS number(s): 77.80.bn, 77.80.Dj, 81.30.Hd

I. INTRODUCTION

The morphotropic phase boundary (MPB), highly sought after in piezoelectric materials, is a phase transition region between competing ferroelectric phases with energy proximity in the phase diagram [1,2]. Low-symmetry phases are commonly observed within the MPBs, bridging phases with different crystal symmetries [3]. Consequently, polarization rotation under external stimuli is much easier in this region, leading to giant electromechanical response. Both chemical doping and strain can induce MPB in lead zirconate titanate (PZT) ferroelectrics. The similarity in the phase transition sequence and corresponding polarization rotation path suggests that hydrostatic pressure and chemical pressure play a similar role in generating MPB [4,5].

$BiFeO_3$ (BFO), a prototype multiferroic, has recently risen as a potential lead-free substitute due to its large ferroelectric polarization that matches up to $PbTiO_3$ [6]. Numerous studies have been devoted to the search for MPBs in BFO-based solid solutions, aiming to reproduce the story of PZT [7,8]. The most notable case is to replace the Bi atom with rare-earth (RE) elements. Due to the chemical pressure induced by the RE substitution, BFO lattice undergoes a structural transformation from rhombohedral $R3c$ to orthorhombic $Pnma$, accompanied by a ferroelectric-antiferroelectric (FE-AFE)-like transition [9–11]. Although early studies did not observe such transition in La-doped BFO thin films [12,13], both theoretical and experimental studies on bulk $Bi_{1-x}La_xFeO_3$ samples strongly suggest a similar polar-antipolar transition region with enhanced dielectric and piezoelectric response [14–17]. Thus, the FE-AFE-like MPB caused by RE doping appears to be universal, with the La doping effect less pronounced in epitaxial thin films.

Inspired by hydrostatic pressure–induced phase transitions in $PbTiO_3$, epitaxial strain is used to continuously tune the ground state of BFO thin films from the bulklike rhombohedral phase to the MPB region with the coexistence of rhombohedral-like (R-like) and tetragonal-like (T-like) phases [18]. Specifically, BFO films on (001)-oriented $LaAlO_3$ (LAO) substrates exhibit tetragonal-rhombohedral (T-R) phase coexistence above certain thickness. Such phase mixture can be electrically driven into pure T-like phase, resulting in giant electromechanical response [19]. Highly distorted crystal lattices with symmetry lowering were discovered in the T-R mixed regions due to a compromise in the mechanical boundary conditions [20,21]. Ideally, upon removing the substrate clamping, the T-R transition can be realized freely under stimuli [22].

Built on the established chemical- and strain-driven MPBs in BFO thin films, one may ask whether we can combine these two effects to achieve a tricritical point between the T-like paraelectric, T-like ferroelectric, and R-like ferroelectric phases with strongly softened lattice and even higher piezoelectricity [23]. Motivated by this hypothesis, highly strained BFO films around the strain-induced MPB were doped with different concentrations of La in this study. As the BFO films grown on LAO substrates exhibit two stages of phase evolution, namely pure T-like phase at small film thickness and mixed phases at large film thickness, the effect of La doping was investigated systematically with the thickness evolution.

II. EXPERIMENTAL METHODS

Stoichiometric $Bi_{1-x}La_xFeO_3$ (BLFO) ceramic targets ($x = 0, 0.05, 0.1, 0.15$) were ablated by a KrF (248 nm) pulsed laser for film deposition on (001)-oriented LAO single-crystalline substrates at 650°C under an oxygen partial pressure of 100 mTorr. The growth rate was fixed at 4 nm/min, and the film thicknesses ranged from 20 to 200 nm. For local electrical switching, a 5-nm conductive $Pr_{0.5}Ca_{0.5}MnO_3$ layer was first deposited as the bottom electrode. Film morphology and corresponding piezoresponse force microscopy (PFM) were obtained on a commercial atomic force microscope (MFP3D, Asylum Research) with Pt/Ir coated probes (force constant

*mailyoulu@gmail.com

†jlwang@ntu.edu.sg

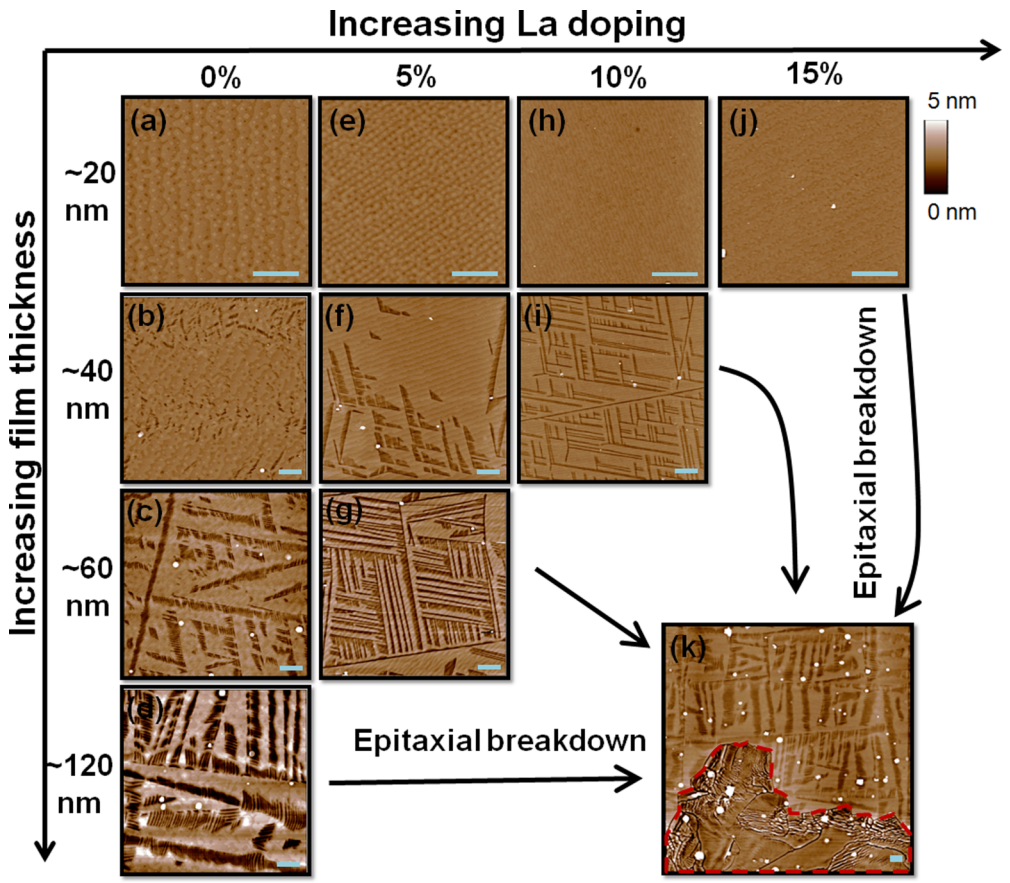

FIG. 1. (Color online) Thickness-dependent evolutions of surface morphologies of BLFO thin films doped with (a–d) no La, (e–g) 5% La, (h, i) 10% La, and (j) 15% La. (k) An example showing partial epitaxial breakdown of the BLFO thin film, as encircled by the red dot line. The scale bars represent 1 μm.

2 N/m). Phase purity and out-of-plane lattice parameters were determined using an x-ray diffractometer (Shimadzu XRD-6000). In-plane polarization hysteresis measurements were carried out on a commercial ferroelectric tester (Precison LC, Radiant Technologies) using planar Pt electrodes patterned by photolithography.

III. EXPERIMENTAL RESULTS

The topographic evolution as the BLFO film thickness increases is displayed in Fig. 1. Pure BFO films exhibit typical stripe mixed-phase region embedded in the T-like matrix above the critical thickness of around 30 nm, below which purely T-like phase is observed with atomic-flat surface. Consistent with previous reports, both the surface fraction and depression of the mixed-phase region increase for thicker films to release the elastic energy without forming extended dislocations [18,24,25]. When La is introduced, the critical thickness for the appearance of the mixed-phase region decreases. Thicker films start to undergo the "epitaxial breakdown" process as the mixed-phase formation itself is not sufficient to release the elastic energy [24]. Nonepitaxial bulklike rhombohedral phase with large cracks appears in the film as shown in Fig. 1(k). Furthermore, more La doping also leads to smaller threshold thickness for epitaxial breakdown.

To gain more insight from the morphological results, we have extracted the relative fractions of T-like matrix and T-R mixed region, and the fraction of epitaxial breakdown area from the topography images. All the results are summarized in Fig. 2, together with the c lattice constants of the BLFO films with varying thicknesses and La doping concentrations. Height histogram data can be extracted from the topographic images, as shown in the inset of Fig. 2(e). The two peaks correspond to the average heights of the mixed-phase region and the T-like matrix, respectively. The fraction of epitaxial breakdown area, fraction of the mixed-phase area, and c lattice constant show a similar trend against La doping; i.e., more La doping leads to lower threshold thickness, as indicated in Figs. 2(d) and 2(e). The c lattice constant of 20-nm-thick BLFO film decreases with more La doping [Fig. 2(f)].

Next, we look into the ferroelectric domain structures of BLFO thin films probed by both in-plane (IP) and out-of-plane (OP) PFM. To reduce the complexity arising from the mixed-phase regions, 20-nm-thick films with mostly T-like phase are first examined, as shown in Fig. 3. All films exhibit atomic-flat surfaces with single unit-cell steps, an indication of step flow growth and fully coherent interface with the substrate. The uniform purple tone found in the OP-PFM images suggests that the out-of-plane polarizations are pointing downward in the as-grown films. Moreover, the out-of-plane polarization is electrically switchable as verified by writing box-in-box

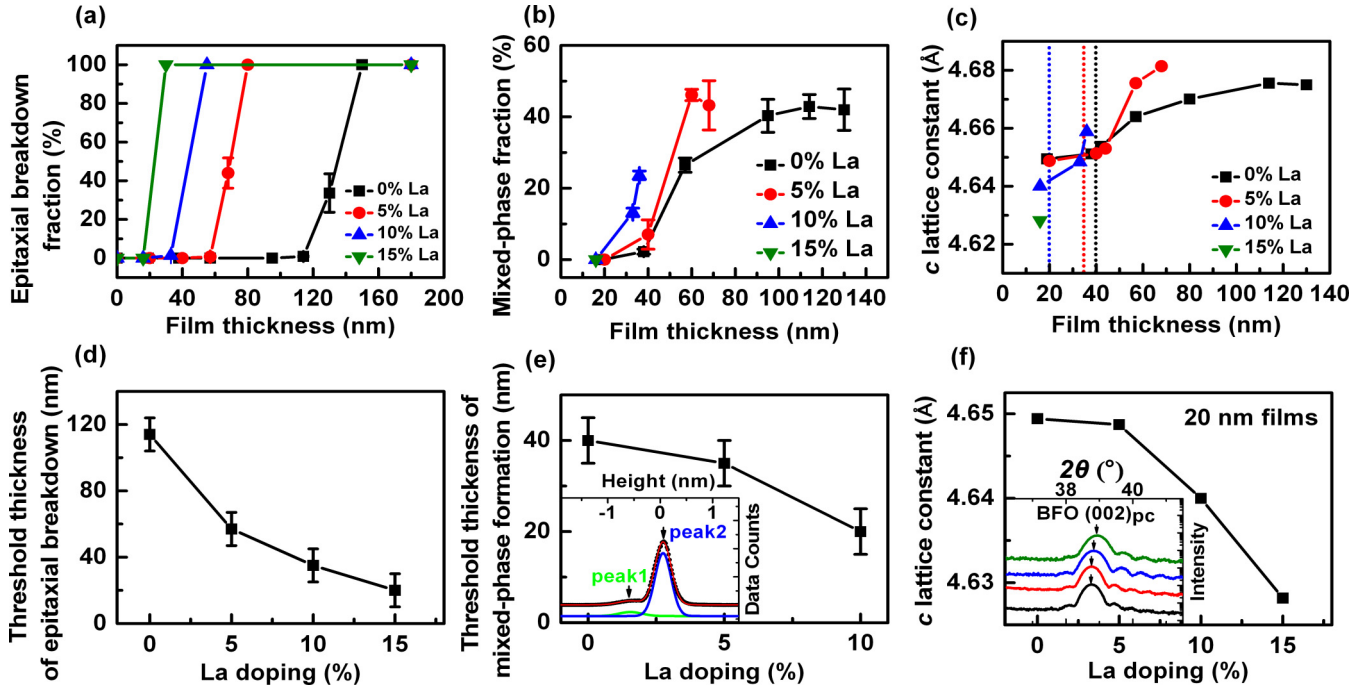

FIG. 2. (Color online) Thickness-dependent evolutions of (a) epitaxial breakdown fraction, (b) mixed-phase fraction, and (c) c lattice constant of BLFO thin films with different La doping concentration. Variations of (d) threshold thickness of epitaxial breakdown, (e) threshold thickness of mixed-phase formation, and (f) c lattice constant of 20-nm-thick film as a function of La doping concentration. The inset of (e) shows an example of the histogram data extracted from the height image. The inset of (f) shows the XRD patterns of 20-nm-thick BLFO films around $(002)_{pc}$ peaks.

patterns using opposite tip bias. Contrarily, the IP-PFM images vary significantly with La doping. The pure BFO film is characterized by highly ordered two-variants stripes with the domain wall running along $[110]_{pc}$ axis, consistent with the monoclinic M_C phase reported previously [26]. Upon replacing 5% Bi by La, the stripe domains persist, however,

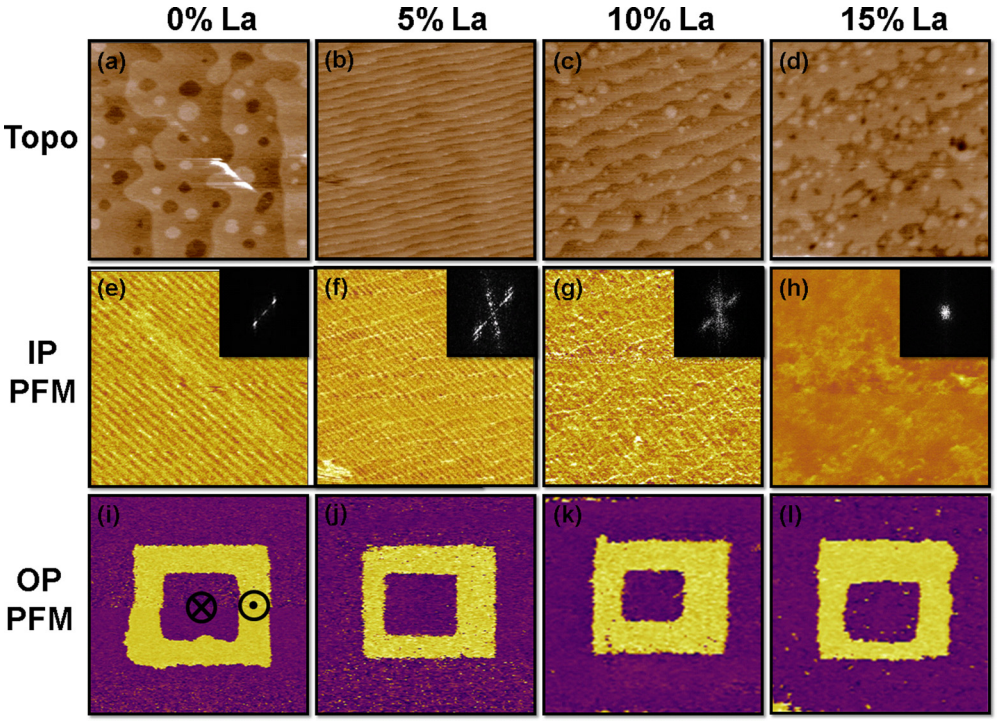

FIG. 3. (Color online) (a–d) Topographies, (e–h) in-plane PFM, and (i–l) out-of-plane PFM images of 20-nm-thick BLFO thin films with different La doping concentrations. The insets of (e–h) are the fast Fourier transform of the corresponding in-plane PFM images. The image sizes of (a–h) and (i–l) are 1 and 2 μm^2, respectively.

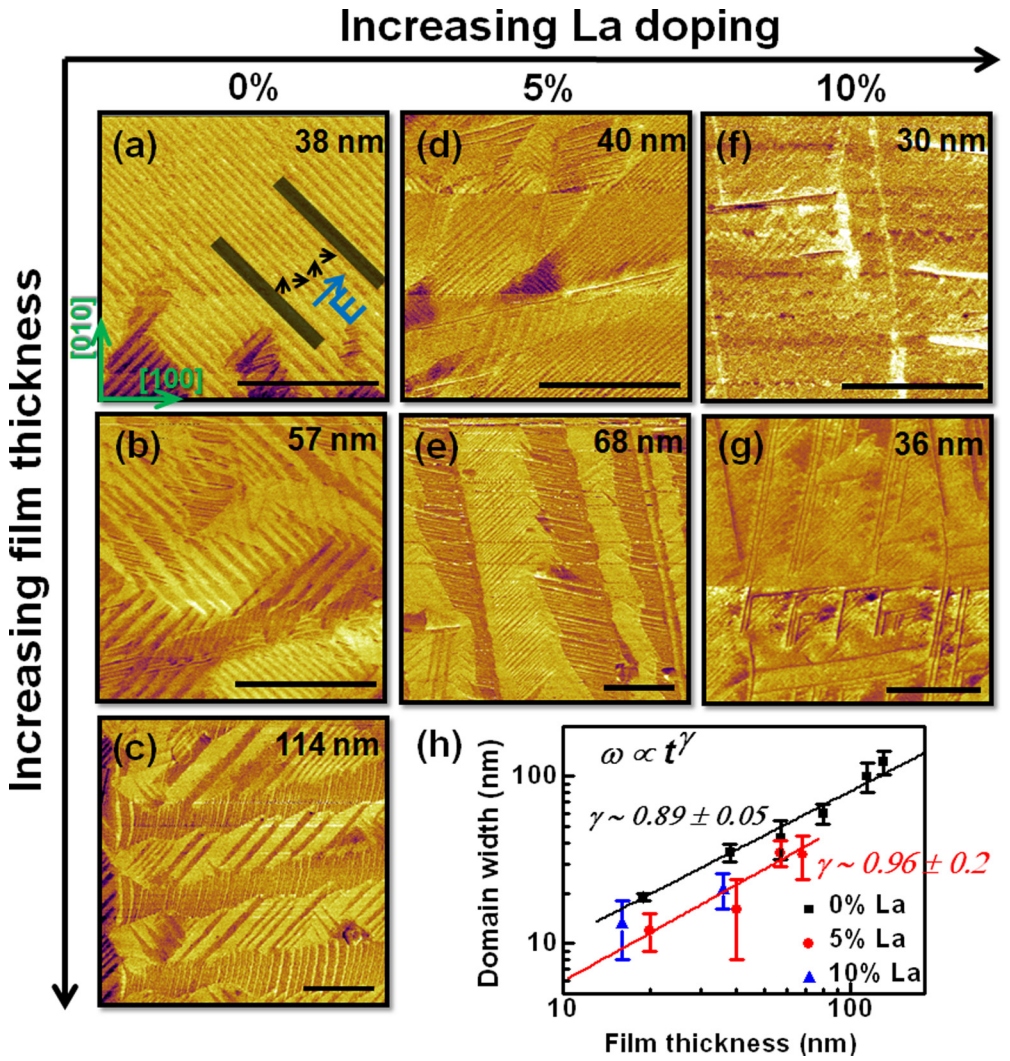

FIG. 4. (Color online) (a)–(g) Thickness-dependent evolutions of in-plane ferroelectric domains of BLFO thin films with different La doping concentrations. (h) Scaling behavior of domain width with regard to film thickness in BLFO thin films. The scale bars are equal to 1 μm.

with reduced domain width. Further La substitution leads to diminishing of the stripe pattern, though a vague trace is still visible. At 15% doping concentration, the stripe pattern completely disappears, leaving no noticeable domain contrast in the IP-PFM image (this is due to the very weak in-plane polarization as discussed below). The ferroelectric domain structures for thicker films are shown in Fig. 4. Although mixed-phase regions appear in these films, the stripe domains of the T-like matrix are still distinctly visible and gradually narrow down and fade out with increasing La doping.

Due to the limited thickness of the BLFO films, direct measurement of out-of-plane polarization is prevented by the large leakage current. Instead, in-plane polarization is measured using planar electrodes with the electric field along the $\langle 110 \rangle_{pc}$ directions [schematically shown in Fig. 4(a)]. Thickness-dependent in-plane remanent polarization (P_r) shows sudden drops for thicker films, which correlates with the appearance of the mixed-phase region [Figs. 5(a) and 5(b)]. Thus, only the hysteresis loops of 20-nm-thick BLFO films with pure T-like phase are used to investigate the effect of La doping. As shown in Fig. 5(c), pure BFO exhibits a well-defined square loop with in-plane P_r of $\sim 23\,\mu C/cm^2$, slightly lower than the value previously reported [27]. A La substitution of 5% results in greatly reduced coercive field, but the P_r value remains. Interestingly, a 10% La-doping sample displays a double-hysteresis loop with the same saturated polarization, which is a signature of antiferroelectriclike behavior. Finally, 15% La doping strongly reduces the saturated polarization, and drives the system towards a paraelectriclike state. To summarize, La doping causes the in-plane polarization to lose its stability by crossing over a double-hysteresis state. In the mean time, the coercive field decreases monotonically. Note that these behaviors are limited to the in-plane polarization component.

IV. DISCUSSION

A. Structural and morphological evolution

The strain-driven MPB of BFO film on LAO substrate has been extensively discussed previously [20,24,28]. Theoretically, it can be considered as the free-energy crossover between the giant axial T-like phase and the R-like phase akin to the bulk

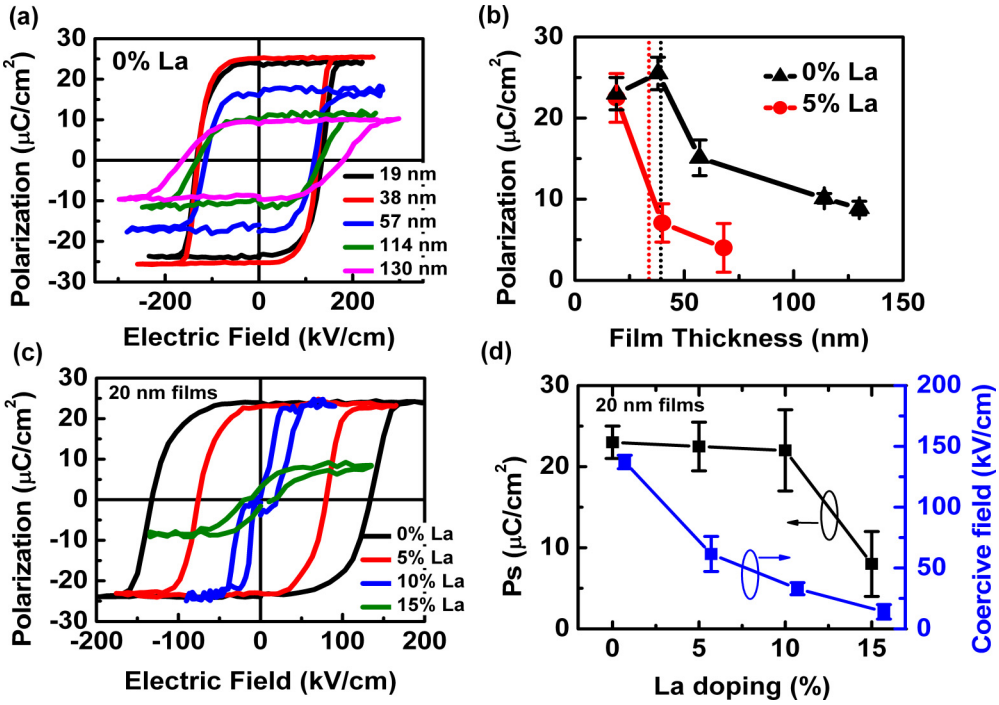

FIG. 5. (Color online) (a) Thickness-dependent in-plane polarization hysteresis loops of highly strained pure BFO. (b) In-plane polarization as a function of film thickness of BLFO films with 0% and 5% La doping. (c) In-plane polarization hysteresis loops of 20-nm-thick BLFO films with different La doping concentrations. (d) Changes of saturated polarization and coercive field as a function of La doping concentrations.

during the relaxation process of the elastic energy. Previous study of BFO films on $NdAlO_3$ ($a \sim 3.747$ Å) indicates that the ground state of the T-like BFO phase has an average in-plane lattice parameter of around 3.76 Å [28]. Consequently, the T-like BFO phase grown on LAO ($a \sim 3.79$ Å) substrate is subject to tensile strain as depicted in Fig. 6(a). At low film thickness, the T-like phase is fully clamped by the substrate. The strain relaxation at this stage is realized through domain twinning [29,30]. This twinning process results in anisotropic in-plane lattice parameters that correlate with the in-plane projection of the polarization, while maintaining the in-plane area unchanged. Therefore, the out-of-plane lattice parameter remains constant, given that the lattice volume is conserved. With increasing thickness, the elastic energy builds up until the critical thickness is reached. However, instead of forming extended defects such as dislocations, the film undergoes spinodal phase separation leading to a mixture of R-like and T-like BFO. The R-phase has a larger in-plane lattice that relieves the tensile strain endured by the T-like phase. Thus, the phase mixture can be considered as a compromise made between T-like and R-like phases to match up with the lattice of the LAO substrate. The two phases share one common in-plane lattice with the defect-free phase boundary lying somewhere close to the orthogonal plane, resulting in a ~4.5° tilting of the crystallographic axis. This situation is analogous to the *a*-*c* domain boundary in tetragonal $PbTiO_3$.

Upon La doping, the *c* lattice constant of the fully coherent 20-nm films decreases despite Bi^{3+} and La^{3+} ions having very similar effective ionic radii (1.17 Å versus 1.16 Å for eightfold coordination [31]). However, this is consistent with other reports of unit-cell shrinking in La-substituted bulk or bulklike BFO samples [14,32,33]. Even though the chemical pressure induced by the La substitution is small compared to other rare-earth elements, it has a huge impact on the thickness-dependent morphology evolution of the mixed-phase BLFO films. Since La doping reduces the lattice parameters of BFO, the tensile strain imposed on the film increases accordingly. Based on the widely accepted model for the misfit accommodation by dislocations in epitaxial films, the critical thickness for the onset of structural relaxation is inversely proportional to the misfit strain experienced by the film [34]. In the mixed-phase BFO system, the formation of dislocation is replaced by the formation of the R-like phase. As a result, more La doping leads to larger misfit tensile strain, and consequently smaller critical thickness for the appearance of mixed phases. A similar trend can be found in the epitaxial breakdown process which involves the strain-relaxation-driven spinodal phase separation during the film growth at high temperature.

The formation of T-R mixed phases, in turn, squeezes the in-plane space of the surrounding T-like phase, causing its lattice to elongate along the out-of-plane direction. As a result, the thickness-dependent evolution of the *c* lattice constant of the T-like phase follows the same trend of the fraction of mixed phases in the film. On the other hand, the shorter *c* axis of the R-like phase causes the surface depression in the mixed-phase region. The average depth is determined by the fraction of the R-like phase in the mixed-phase region. As shown in Fig. 6(c), the average depth of the mixed-phase region in BLFO films with different La concentrations exhibits a common linear relationship with the film thickness. The slope of the fitted curve (~0.022) represents the average strain along the *c* axis. Considering the situation with complete R-like phase, the out-of-plane strain is calculated by $(c_{\mathrm{T-like}} - c_{\mathrm{R-like}})/c_{\mathrm{T-like}}$ to be ~0.105, where $c_{\mathrm{T-like}}$ and $c_{\mathrm{R-like}}$ are the out-of-plane lattice

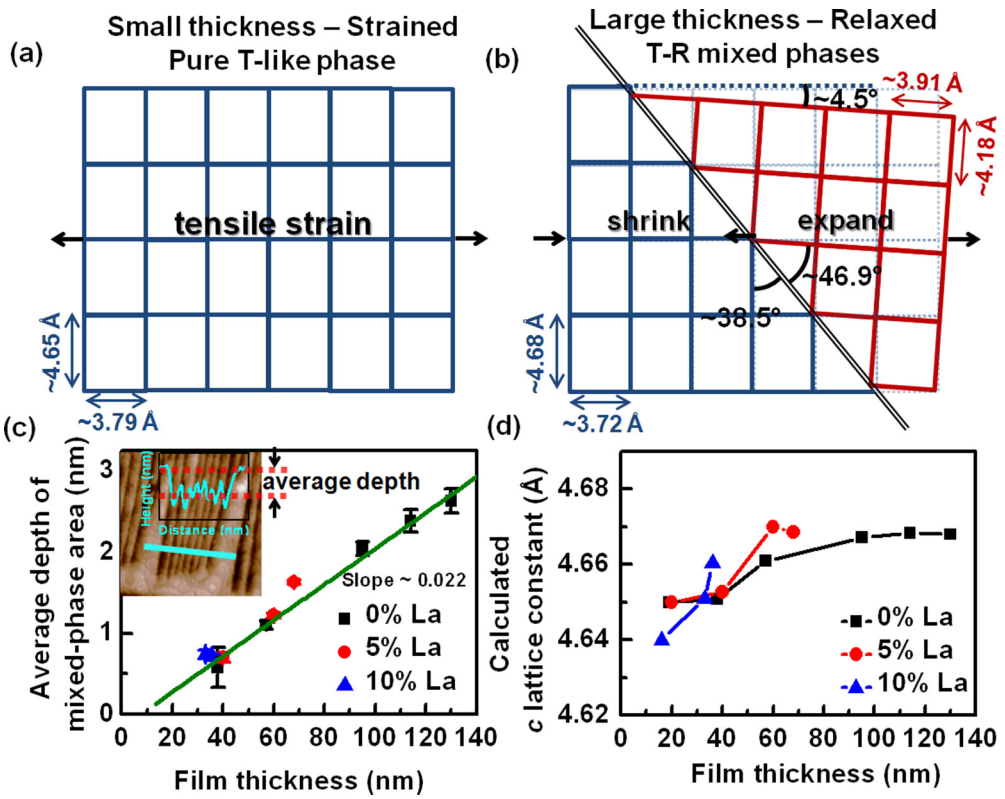

FIG. 6. (Color online) Schematic drawings showing the lattice distortion of BFO thin films grown on LAO substrate at (a) small thickness with purely T-like phase and (b) large thickness with relaxed T-R mixed phases. (c) Average depth of the mixed-phase region as a function of film thickness showing a linear relationship. The inset shows the line profile around the striped mixed-phase region that indicates the average depth. (d) Calculated c lattice constant evolutions against film thickness for different La doping level.

parameters of T-like and R-like phases, respectively. Thus, the volume fraction of the R-like phase in the T-R phase mixture is estimated to be around 20%, which can be multiplied by the fraction of mixed-phase area [Fig. 2(b)] to get the fraction of R-like phase in the whole film. The shrinkage of the in-plane lattice of the T-like phase can subsequently be resolved by matching the average lattice of T-like and R-like phases to the LAO substrate. Finally, the elongation of the c lattice constant of the T-like phase is calculated through the Poisson's effect:

$$\nu = \frac{1}{1 - 2\varepsilon_{xx}/\varepsilon_{zz}},$$

where ν is the poisson ratio, and ε_{xx} and ε_{zz} are the in-plane and out-of-plane biaxial strain, respectively. The calculated c lattice constant shown in Fig. 6(d) reproduces the experimental results in Fig. 2(c).

B. Ferroelectric domain evolution

The switchable out-of-plane polarization as demonstrated in the OP-PFM images suggests that the T-like BLFO films remain ferroelectric up to 15% La doping. The IP-PFM images, on the contrary, show gradually diminishing contrast of the stripe domains. The insets of Figs. 3(e)–3(h) show the corresponding two-dimensional (2D) fast Fourier transform (2D FFT) images. Two distinct peaks can be seen in pure BFO film, indicating periodic stripe domains along the direction normal to the domain walls. A 5% sample shows similar modulation with shorter period, or smaller domain width. The peaks appearing along the orthogonal direction are due to the topographic artifact induced by the surface steps. A strong diffusion of the peaks can be observed when 10% La is introduced, implying the loss of the periodicity of the stripe domains. Lastly, 15% film no longer displays periodic stripe domains.

Statistically, the degree of the order in a system can be evaluated using the autocorrelation transformation [35],

$$\langle C(r_1,r_2)\rangle = \langle D(x,y)D(x+r_1,y+r_2)\rangle,$$

where $D(x, y)$ is the magnitude of piezoresponse in the 2D PFM images at location (x, y), and the polarization-polarization correlation function $\langle C(r_1,r_2)\rangle$ means the average over all possible pairs in the 2D matrix that are separated by the vector (r_1, r_2). The autocorrelation images for the IP-PFM patterns of BLFO films are shown in Figs. 7(a)–7(d). Clearly, the periodic stripe pattern gradually vanishes at higher La doping concentrations, resembling that of the IP-PFM image. The corresponding line profiles of the autocorrelation functions along the $\langle 110\rangle_{pc}$ axis are also presented below [Figs. 7(e)–7(h)]. Nonvanishing oscillation for pure BFO at large distance is an indication of long-range order. Five percent La doping greatly reduces the amplitude of the oscillation in the autocorrelation function, whereas more La causes exponential decay to zero, suggesting increasing disorder in in-plane polarization.

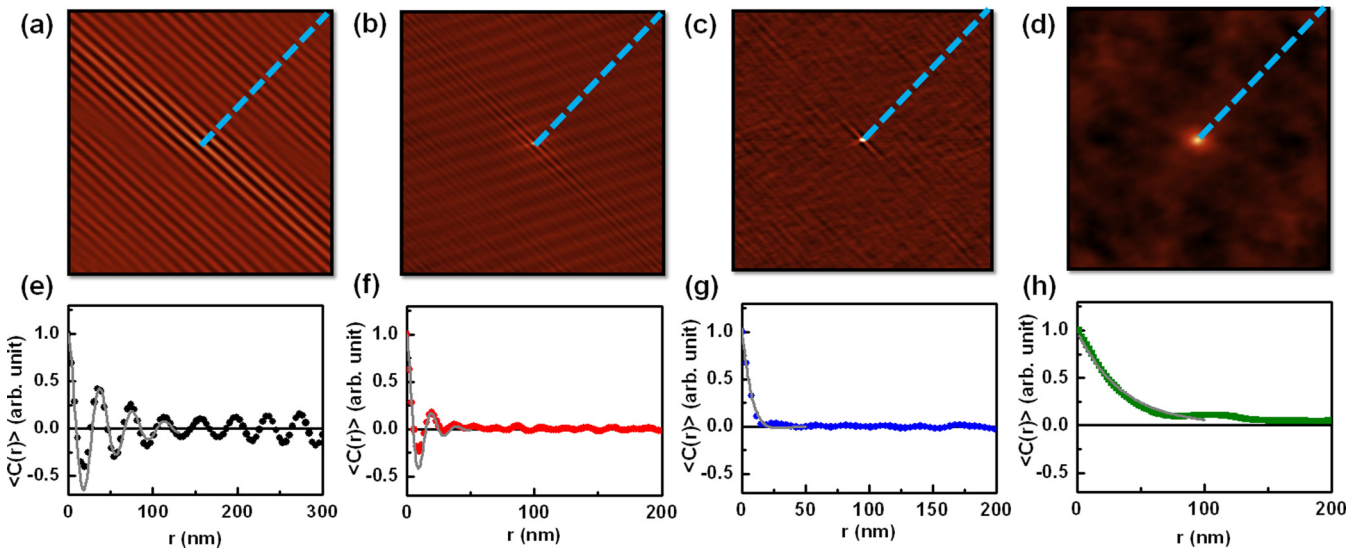

FIG. 7. (Color online) Autocorrelation images of Figs. 3(e)–3(h). (e–h) Corresponding line profiles as depicted by the dashed lines in (a–d). Solid lines are fittings based on long-range order.

Thickness-dependent evolution of the in-plane ferroelectric domain structures for different La doping essentially shows similar order-disorder transition. The domain width W of the BLFO films with different thickness d follows the power law $W \propto d^{\gamma}$, with γ close to 0.9. This value differs notably from the Landau-Lifshitz-Kittel (LLK) scaling law ($\gamma = 0.5$) [36], but agrees with previous reports on T-like BFO films [28,29]. It should be noted that the classical square root law is only valid when the film thickness is much larger than the domain width. A strong deviation can be observed if the film thickness becomes comparable to the domain size [37]. Particularly, the LLK law predicts $W \propto (\sigma d)^{1/2}$ with σ being the domain wall energy [38]. However, during the thickness-dependent strain-relaxation process, the shear distortion of the T-like phase increases with the film thickness [30]. Therefore, the elastic domain wall energy is in fact a function of the film thickness, which causes the exponential term γ to be larger than 0.5 as seen in our case. Likewise, La doping further reduces the in-plane lattice anisotropy and the shear distortion [39–41], resulting in even smaller domain sizes compared with pure BFO. Furthermore, the micrometer-long mixed-phase stripes observed in La-doped BFO films may also be attributed to the reduction of lattice distortion together with elastic domain boundary energy due to the chemical pressure [41].

C. Ferroelectric polarization evolution

Thickness-dependent in-plane polarization measurements indicate that the formation of the mixed-phase region strongly impedes the in-plane polarization switching. This is not surprising, as the in-plane polarization components within the mixed-phase region are constrained by the elastic boundaries and cannot rotate freely under external field. For film without the mixed-phase region, the in-plane polarization can be measured with excellent agreement with the local domain structures. The key finding here is the weakening of the in-plane polarization upon La doping, including the reduction of the coercive field at first, followed by the appearance of double-hysteresis behavior, and finally the vanishing of the switchable in-plane polarization. The free energy of in-plane polarization versus La concentration is schematically shown in Fig 8(a), which can be viewed as a first-order ferroelectric-paraelectric phase transition. The reduced coercive field can be explained by the decrease of the energy barrier in the potential double well. However, it should be noted that such a transition only occurs for the in-plane component of the polarization. The out-of-plane polarization remains robust up to 15% La doping. Combining these two facts, a polarization-rotation scenario can be envisaged as illustrated in Fig. 8(b). The T-like M_C phase has a small in-plane polarization component which is destabilized by the La substitution, eventually leading to a quasitetragonal phase with negligible in-plane polarization (further detailed structural analysis is required to verify this). The intermediate stage is characterized by a state of polar instability, in which the in-plane polar state can be induced by the external electric field as manifested by the double-hysteresis behavior. The macroscopic in-plane polarization measurements are completely in agreement with the domain structures as seem by IP-PFM images, where the ferroelectric order gradually diminshes upon La doping. This result echoes a previous report of polarization rotation in bulklike rhombohedral BFO thin films induced by Sm substitution, signifying the universality of the chemical pressure effect in A-site-doped BFO [42]. The effect can be understood by the switching off of lone-pair activity of Bi^{3+}, namely, the driving force of the ferroelectricity [7]. Particularly, on the $(001)_{pc}$-oriented substrates, the switching off of ferroelecticity first takes place in the in-plane direction as a result of the biaxial in-plane strain, rendering the monoclinic distortion angle closer to 90° and a reduction of the in-plane lattice anisotropy. Further doping will lead to the destabilization of the out-of-plane polarization, inducing a global ferroelectric-paraelectric phase transition. However, in our T-like BFO phase, robust out-of-plane ferroelectricity is observed up to 15% La doping, while increasing doping does not produce a global paraelectric phase. Instead, the lattice collapses into the

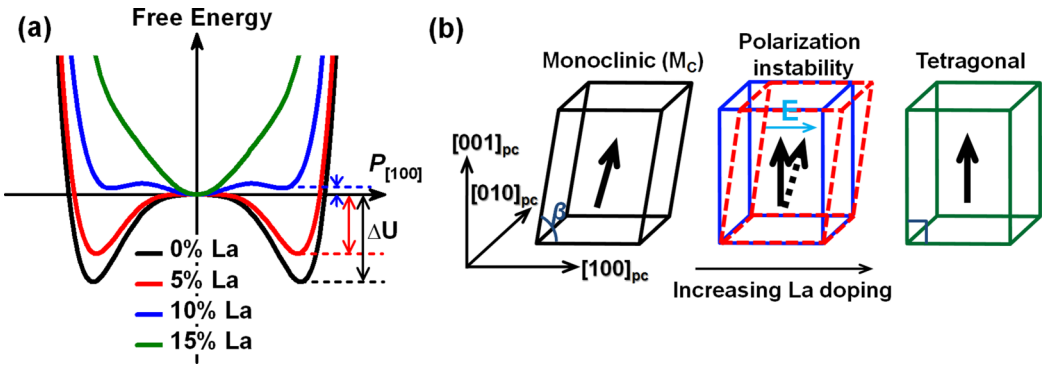

FIG. 8. (Color online) (a) Evolution of the free energy of in-plane polarization in BLFO thin films with different La doping concentrations. (b) A schematic showing the changes of structure and ferroelectric order against increasing La doping.

R-like phase with complete strain relaxation. In other words, the T-like ferroelectric-paraelectric transition does not occur in the strain-composition phase diagram at room temperature. Therefore, a tricritical point between T-like ferroelectric, T-like paraelectric, and R-like ferroelectric phases cannot be achieved to enhance the electromechanical response.

V. CONCLUSION

In this study, structural, morphological, and ferroelectric evolutions of the highly strained BLFO thin films with film composition and thickness are systematically investigated. It is found that La substitution induces non-negligible chemical pressure that strongly affects the mixed-phase formation upon strain relaxation. Furthermore, the La doping destabilizes the in-plane polarization component and causes the polarization to rotate completely out of the film plane, which is verified by both macroscopic in-plane polarization measurements and local in-plane ferroelectric domain imaging. These findings support the universality of the polar instability induced by chemical substitution of the Bi^{3+}, whose stereochemical activity is the source of ferroelectric order in BFO.

ACKNOWLEDGMENTS

The authors acknowledge the support from Nanyang Technological University and Ministry of Education of Singapore under Project No. ARC 32/13. Partial support from National Research Foundation of Singapore under Project No. NRF-CRP5-2009-04 is also acknowledged.

[1] B. Noheda, Curr. Opin. Solid State Mater. Sci. **6**, 27 (2002).
[2] J. Rödel, W. Jo, K. T. P. Seifert, E.-M. Anton, T. Granzow, and D. Damjanovic, J. Am. Ceram. Soc. **92**, 1153 (2009).
[3] B. Noheda and D. E. Cox, Phase Transitions **79**, 5 (2006).
[4] H. Fu and R. E. Cohen, Nature **403**, 281 (2000).
[5] M. Ahart, M. Somayazulu, R. E. Cohen, P. Ganesh, P. Dera, H.-k. Mao, R. J. Hemley, Y. Ren, P. Liermann, and Z. Wu, Nature **451**, 545 (2008).
[6] J. Wang, J. B. Neaton, H. Zheng, V. Nagarajan, S. B. Ogale, B. Liu, D. Viehland, V. Vaithyanathan, D. G. Schlom, U. V. Waghmare, N. A. Spaldin, K. M. Rabe, M. Wuttig, and R. Ramesh, Science **299**, 1719 (2003).
[7] G. Catalan and J. F. Scott, Adv. Mater. **21**, 2463 (2009).
[8] C.-H. Yang, D. Kan, I. Takeuchi, V. Nagarajan, and J. Seidel, Phys. Chem. Chem. Phys. **14**, 15953 (2012).
[9] S. Fujino, M. Murakami, V. Anbusathaiah, S.-H. Lim, V. Nagarajan, C. J. Fennie, M. Wuttig, L. Salamanca-Riba, and I. Takeuchi, Appl. Phys. Lett. **92**, 202904 (2008).
[10] D. Kan, L. Pálová, V. Anbusathaiah, C. J. Cheng, S. Fujino, V. Nagarajan, K. M. Rabe, and I. Takeuchi, Adv. Funct. Mater. **20**, 1108 (2010).
[11] A. Y. Borisevich, E. A. Eliseev, A. N. Morozovska, C. J. Cheng, J. Y. Lin, Y. H. Chu, D. Kan, I. Takeuchi, V. Nagarajan, and S. V. Kalinin, Nat. Commun. **3**, 775 (2012).
[12] C.-J. Cheng, D. Kan, V. Anbusathaiah, I. Takeuchi, and V. Nagarajan, Appl. Phys. Lett. **97**, 212905 (2010).
[13] D. Kan, C.-J. Cheng, V. Nagarajan, and I. Takeuchi, J. Appl. Phys. **110**, 014106 (2011).
[14] D. A. Rusakov, A. M. Abakumov, K. Yamaura, A. A. Belik, G. Van Tendeloo, and E. Takayama-Muromachi, Chem. Mater. **23**, 285 (2010).
[15] I. O. Troyanchuk, D. V. Karpinsky, M. V. Bushinsky, V. A. Khomchenko, G. N. Kakazei, J. P. Araujo, M. Tovar, V. Sikolenko, V. Efimov, and A. L. Kholkin, Phys. Rev. B **83**, 054109 (2011).
[16] O. E. González-Vázquez, J. C. Wojdeł, O. Diéguez, and J. Íñiguez, Phys. Rev. B **85**, 064119 (2012).
[17] D. V. Karpinsky, I. O. Troyanchuk, M. Tovar, V. Sikolenko, V. Efimov, and A. L. Kholkin, J. Alloys Compd. **555**, 101 (2013).
[18] R. J. Zeches, M. D. Rossell, J. X. Zhang, A. J. Hatt, Q. He, C.-H. Yang, A. Kumar, C. H. Wang, A. Melville, C. Adamo, G. Sheng, Y.-H. Chu, J. F. Ihlefeld, R. Erni, C. Ederer, V. Gopalan, L. Q. Chen, D. G. Schlom, N. A. Spaldin, L. W. Martin *et al.*, Science **326**, 977 (2009).
[19] J. X. Zhang, B. Xiang, Q. He, J. Seidel, R. J. Zeches, P. Yu, S. Y. Yang, C. H. Wang, Y.-H. Chu, L. W. Martin, A. M. Minor, and R. Ramesh, Nat. Nanotechnol. **6**, 98 (2011).
[20] Z. Chen, S. Prosandeev, Z. L. Luo, W. Ren, Y. Qi, C. W. Huang, L. You, C. Gao, I. A. Kornev, T. Wu, J. Wang, P. Yang, T. Sritharan, L. Bellaiche, and L. Chen, Phys. Rev. B **84**, 094116 (2011).
[21] A. R. Damodaran, C.-W. Liang, Q. He, C.-Y. Peng, L. Chang, Y.-H. Chu, and L. W. Martin, Adv. Mater. **23**, 3170 (2011).

[22] J. X. Zhang, X. X. Ke, G. Y. Gou, J. Seidel, B. Xiang, P. Yu, W.-I. Liang, A. M. Minor, Y.-H. Chu, G. Van Tendeloo, X. B. Ren, and R. Ramesh, Nat. Commun. **4**, 2768 (2013).
[23] W. Liu and X. Ren, Phys. Rev. Lett. **103**, 257602 (2009).
[24] A. R. Damodaran, S. Lee, J. Karthik, S. MacLaren, and L. W. Martin, Phys. Rev. B **85**, 024113 (2012).
[25] H.-J. Liu, C.-W. Liang, W.-I. Liang, H.-J. Chen, J.-C. Yang, C.-Y. Peng, G.-F. Wang, F.-N. Chu, Y.-C. Chen, H.-Y. Lee, L. Chang, S.-J. Lin, and Y.-H. Chu, Phys. Rev. B **85**, 014104 (2012).
[26] Z. Chen, Z. Luo, C. Huang, Y. Qi, P. Yang, L. You, C. Hu, T. Wu, J. Wang, C. Gao, T. Sritharan, and L. Chen, Adv. Funct. Mater. **21**, 133 (2011).
[27] Z. Chen, X. Zou, W. Ren, L. You, C. Huang, Y. Yang, P. Yang, J. Wang, T. Sritharan, L. Bellaiche, and L. Chen, Phys. Rev. B **86**, 235125 (2012).
[28] C.-S. Woo, J. H. Lee, K. Chu, B.-K. Jang, Y.-B. Kim, T. Y. Koo, P. Yang, Y. Qi, Z. Chen, L. Chen, H. C. Choi, J. H. Shim, and C.-H. Yang, Phys. Rev. B **86**, 054417 (2012).
[29] Z. Luo, Z. Chen, Y. Yang, H.-J. Liu, C. Huang, H. Huang, H. Wang, M.-M. Yang, C. Hu, G. Pan, W. Wen, X. Li, Q. He, T. Sritharan, Y.-H. Chu, L. Chen, and C. Gao, Phys. Rev. B **88**, 064103 (2013).
[30] C. J. M. Daumont, S. Farokhipoor, A. Ferri, J. C. Wojdeł, Jorge Íñiguez, B. J. Kooi, and B. Noheda, Phys. Rev. B **81**, 144115 (2010).
[31] R. Shannon, Acta Crystallogr., Sect. A **32**, 751 (1976).
[32] I. O. Troyanchuk, D. V. Karpinsky, M. V. Bushinsky, O. S. Mantytskaya, N. V. Tereshko, and V. N. Shut, J. Am. Ceram. Soc. **94**, 4502 (2011).
[33] J.-H. Lee, H. J. Choi, D. Lee, M. G. Kim, C. W. Bark, S. Ryu, M.-A. Oak, and H. M. Jang, Phys. Rev. B **82**, 045113 (2010).
[34] J. W. Matthews and A. E. Blakeslee, J. Cryst. Growth **27**, 118 (1974).
[35] V. V. Shvartsman, B. Dkhil, and A. L. Kholkin, Annu. Rev. Mater. Res. **43**, 423 (2013).
[36] G. Catalan, H. Béa, S. Fusil, M. Bibes, P. Paruch, A. Barthélémy, and J. F. Scott, Phys. Rev. Lett. **100**, 027602 (2008).
[37] C. W. Huang, Z. H. Chen, and L. Chen, J. Appl. Phys. **113**, 094101 (2013).
[38] C. W. Huang, L. Chen, J. Wang, Q. He, S. Y. Yang, Y. H. Chu, and R. Ramesh, Phys. Rev. B **80**, 140101 (2009).
[39] W. Chen, W. Ren, L. You, Y. Yang, Z. Chen, Y. Qi, X. Zou, J. Wang, T. Sritharan, P. Yang, L. Bellaiche, and L. Chen, Appl. Phys. Lett. **99**, 222904 (2011).
[40] H. M. Christen, J. H. Nam, H. S. Kim, A. J. Hatt, and N. A. Spaldin, Phys. Rev. B **83**, 144107 (2011).
[41] K.-E. Kim, B.-K. Jang, Y. Heo, J. Hong Lee, M. Jeong, J. Y. Lee, J. Seidel, and C.-H. Yang, NPG Asia Mater. **6**, e81 (2014).
[42] D. Kan, V. Anbusathaiah, and I. Takeuchi, Adv. Mater. **23**, 1765 (2011).